Pictorial Essay

Incremental Value of Magnetic Resonance Imaging in Further Characterizing Hypodense Mediastinal and Paracardiac Lesions Identified on Computed Tomography

Abhishek Chaturvedi, Chris Gange, Hakan Sahin, Apeksha Chaturvedi

Department of Imaging Science, University of Rochester Medical Center, Rochester, NY, USA

ABSTRACT

Mediastinal and paracardiac lesions are usually first diagnosed on a chest radiograph or echocardiogram. Often, a computed tomography is obtained to further delineate these lesions. CT may be suboptimal for evaluation of enhancement characteristics and direct extension into the adjacent mediastinal structures. With its intrinsic superior soft-tissue characterization, magnetic resonance imaging (MRI) can better delineate these lesions, their internal tissue characteristics, and identify adhesion/invasion into adjacent structures. This pictorial essay provides a brief synopsis of the key MRI sequences and their utility in further characterizing mediastinal and paracardiac lesions.

KEYWORDS: *Magnetic resonance imaging, mediastinal, paracardiac, pericardial*

INTRODUCTION

Mediastinal and paracardiac lesions, whether congenital or acquired, are usually first diagnosed on a chest radiograph or echocardiogram. Often, a computed tomography (CT) is obtained to further delineate these lesions. Such a CT is commonly obtained as single venous phase acquisition due to the radiation risk inherent with CT. Although CT is superior to radiographs towards documenting the lesion and its effect on surrounding structures, evaluation of enhancement characteristics and direct extension into the adjacent mediastinal structures leaves much to be desired. With its intrinsic superior soft-tissue characterization, magnetic resonance (MR) can better delineate these lesions, their internal tissue characteristics, and identify adhesion/invasion into adjacent structures. Even though multidetector CT continues to be the modality of choice for identification of pericardial calcifications, magnetic resonance imaging (MRI) is the best imaging modality for comprehensive examination of the paracardiac/pericardial abnormalities and their impact on cardiac function such as pericardial constriction.[1,2] Lessons learnt from neuroradiologic, cardiac, and abdominal applications of MRI can be used to tailor mediastinal MR for such paracardiac lesions identified on thoracic CT.

There are excellent reviews on the evaluation of pericardial thickness, constriction,[1,3] and mediastinal cystic lesions[4] in the literature. The purpose of this article is not to describe these but to describe the incremental value of MRI in further characterizing such mediastinal or paracardiac lesions which may appear hypodense on CT but the measured attenuation is more than simple fluid. On CT distinguishing their organ of origin can sometimes be difficult: do they originate from the pericardium, adjacent mediastinum or adjacent pleura/lung. In addition, identifying encasement and invasion of malignant lesions can be suboptimal on CT. Thus, MR imaging in this subset of cases can provide important information, which has additional diagnostic and prognostic implications.

Address for correspondence: Dr. Abhishek Chaturvedi, Department of Imaging Science, University of Rochester Medical Center, P.O. Box No. 648, 601 Elmwood Ave, Rochester, 14642, NY, USA. E-mail: toabhic@gmail.com

How to cite this article: Chaturvedi A, Gange C, Sahin H, Chaturvedi A. Incremental Value of Magnetic Resonance Imaging in Further Characterizing Hypodense Mediastinal and Paracardiac Lesions Identified on Computed Tomography. J Clin Imaging Sci 2018;8:10. Available FREE in open access from: http://www.clinicalimagingscience.org/text.asp?2018/8/1/10/227124

ANATOMY OF THE MEDIASTINUM AND PERICARDIUM

For the purpose of formulating differential diagnoses, mediastinum can be divided into 3-4 compartments, but there are no clear-cut physical boundaries that would limit disease.[5] International Thymic Malignancy Interest Group -modified classification of mediastinal compartments is useful for cross-sectional imaging and includes prevascular, visceral, and paravertebral compartments.[6] Contents of the visceral or middle compartment include esophagus, trachea, thoracic duct, and all the structures within the pericardium (heart, aorta, and pulmonary artery). Pericardium is a conical fibroserous sac surrounding the heart and origins of the large blood vessels[7] [Figure 1, illustration]. Macroscopically, it is composed of three layers-outer fibrous and inner double- layered serous. Serous pericardium includes the visceral pericardium/epicardium and the outer parietal pericardium which is adherent to the outer fibrous layer.[8,9] The serosa forms a complete sac filled with up to 50 mL of plasmatic ultrafiltrate and is separated from the heart by loose epicardial connective tissue and a single layer of mesothelial cells.[1]

MAGNETIC RESONANCE IMAGING SEQUENCES

The key MRI sequences useful for characterizing mediastinal, pericardial, and paracardial (lesions which are adjacent to but outside the pericardium) are described in Table 1. Use of electrocardiogram (ECG) gating and respiratory breath hold results in decreased motion artifacts. Cysts and benign thymic lesions and invasion of mediastinum/chest wall can often be characterized without the use of intravenous gadolinium-based contrast. This is especially important in patients who cannot receive contrast for either CT or MRI (renal failure, history of anaphylaxis to previous contrast medium administration, etc.). Contrast-enhanced images are useful to further characterize the enhancement pattern of solid lesions and can aid differentiation of benign from malignant lesions. Each sequence adds value and helps solve the jigsaw puzzle that such lesions may present. Depending on the clinical question to be answered, sequences can be added or removed [Figure 2, Flowchart]. Respiratory navigator may be used in patients with dyspnea and inability to hold breath. Arrhythmia rejection or a peripheral pulse unit may be used in patients with inefficient ECG gating. Spin echo sequences can be tried in the presence of susceptibility artifacts due to the presence of metal such as sternal wires, prosthetic valves. Modification of metal suppression sequences as described for musculoskeletal imaging can sometimes also be useful.[10]
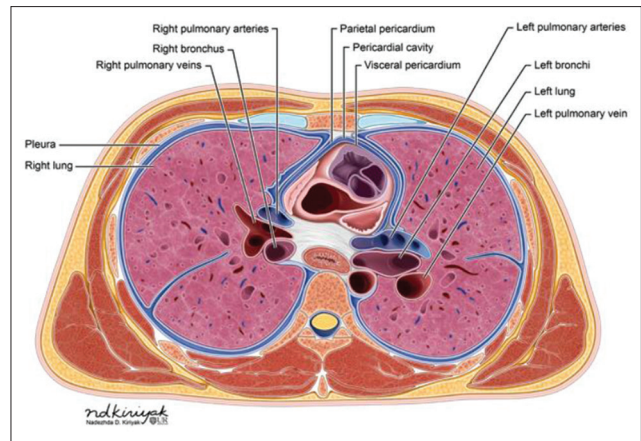
Figure 1: Illustration demonstrating the normal anatomy of the mediastinum, pericardium, and adjacent paracardiac region.

MEDIASTINUM AND THE PARACARDIAC REGION

Paracardiac and mediastinal lesions can be originate from the mediastinum or adjacent pleura and lungs. They can be benign or malignant. It can sometimes be difficult to identify the site of origin of these lesions on CT. Key imaging characteristics that help in characterizing these as benign or malignant are presented in Tables 2 and 3 and also explained in the individual figure legends. This brief pictorial essay describes how different MR sequences can be used to further characterize hypodense mediastinal and paracardiac lesions seen on CT with measured attenuation more than simple fluid (about 20 HU). The MR scan obtained for such cases can be tailored to lesion being evaluated, not all cases need to be scanned using all the sequences [Figure 2, flowchart].

T1 WEIGHTED

T1-weighted (T1W) sequences depend on longitudinal relaxation and can be obtained as spin echo or fast spin-echo. These require breath holding in end inspiration or end expiration. Images can also be obtained with ECG gating with late diastolic acquisition to reduce cardiac motion artifacts. Protein-rich contents, fat, melanin, and blood are bright on such images. These are usually obtained as inversion recovery to remove signal from moving particles such as blood (Black Blood). Bronchogenic cysts can appear hyperintense to muscle due to the presence of protein, mucoid, or hemorrhagic material.[4,11] Metastases from melatonic melanoma [Figure 3] can also appear hyperintense.[12,13] Fat-containing lesions such as lipoma, liposarcoma also appear hyperintense on such images. Epicardial fat deposits can be seen in obese individuals and are 3–4 times more prevalent along the right ventricle compared to the left ventricle.[14] Pericardial hematoma [Figure 4] appears hyperintense on T1W images.[15] Constrictive pericarditis is characterized

Table 1: Different pulse sequence useful on MRI in characterizing mediastinal and pericardial Lesions. The suggested imaging parameters are for a 1.5 T MRI (these may also differ on different vendor platforms)

Sequence	Plane	Parameters (1.5 T) FOV, matrix, thickness, gap, TR, TE	Advantage	Others
Bright Blood Localizer	Axial, Sagittal, and Coronal	420 mm 160 × 160 10 mm, overlap TR1015 mm TE 79 mm	Anatomy and planning subsequent views	Ensure the surface coil is centered over the region being evaluated
Dark Blood: T1	Axial or Double oblique	350-420, 320 × 160 4 mm, overlap TR 1000 mm TE 22 mm	Fat, Protenacious fluid, blood are hyperitense	Add STIR/SPIR to look for macroscopic fat, bone marrow edema
Dark Blood: T2	Axial or Double oblique	350-380 242 × 192 6-8 mm, No Gap TR 1300-6666 mm TE 88-810 mm	Edema/Inflammation vs. fibrous tissue or blood products	Add fat saturation pre-pulse to identify macrospoic fat Heavy T2: confirm contents to be fluid
Bright Blood: SSFP	Axial or Double oblique	350-380 242 × 192 6-8 mm, No Gap TR 2.5-3 mm TE 1.3 mm	Cine SSFP to identify focal invasion	Unbalanced: less affected by susceptibility artifacts
In/Out	Axial or Double oblique	350-420 320 × 160 6-8 mm, No Gap TR 6.7 mm TE 2-4 mm	Presence of microscopic fat	Useful for thymic hyperplasia
Real Time	Double oblique, sagittal or coronal	350-380 128 × 128 6-8 mm, No Gap TR 2.2 mm TE 1.1 mm	Adherence to cardiac chambers or vessels, chest wall invasion	Confirm adequate inspiratory effort by evaluating diaphragm motion
Diffusion ADC Map	Axial or Double oblique*	380-400 192 × 192 8 mm, No Gap TR 3900 mm TE 76 mm	Restricted diffusion of water within lesions (hypercellular or thick, tenacious fluid abscess, clotted blood)	Three B values: <50, 100, >500 s/mm2 Exclude 0 images for ADC calculation
Contrast Enhanced	4 phases Axial: Precontrast Arterial Venous Delayed	350-420 320 × 160 4 mm, overlap TR 3.8 mm TE 1.8 mm	Post processed subtraction enables discernment of enhancement within a T1-hyperintense lesion	Time signal intensity graphs can be used to evaluate contrast kinetics when resting perfusion is used
Delayed Contrast Enhanced	Axial or Double oblique	350-420 320 × 160 4 mm, overlap TR 5.9 mm TE 1.3 mm	Fibrosis, thrombus, hematoma	Longer inversion time useful to confirm thrombus

Scan time can be decreased by limiting the Z axis coverage over the lesion only. On a 3 T, frequency scout may be needed for SSFP sequences. *Double oblique: This imaging plane is prescribed from axial, sagittal or coronal planes (identify the lesion and its suspected plane of invasion into the mediastinum). The double oblique plane is prescribed by planning the acquisition perpendicular or parallel to the site of suspected invasion

by increased pericardial thickness leading to impaired ventricular filling with elevated intraventricular pressures. Pericardial constriction/thickening from such hematomas can be evaluated by ECG gated cine MRI [Video 1] which identifies diminished anterior-posterior diameter of the heart, collapse of the right ventricle, or right atrium during diastole. Right ventricular filling normally increases on inspiration. Real-time cine sequence performed during deep inspiration can identify paradoxical motion of the interventricular septum towards
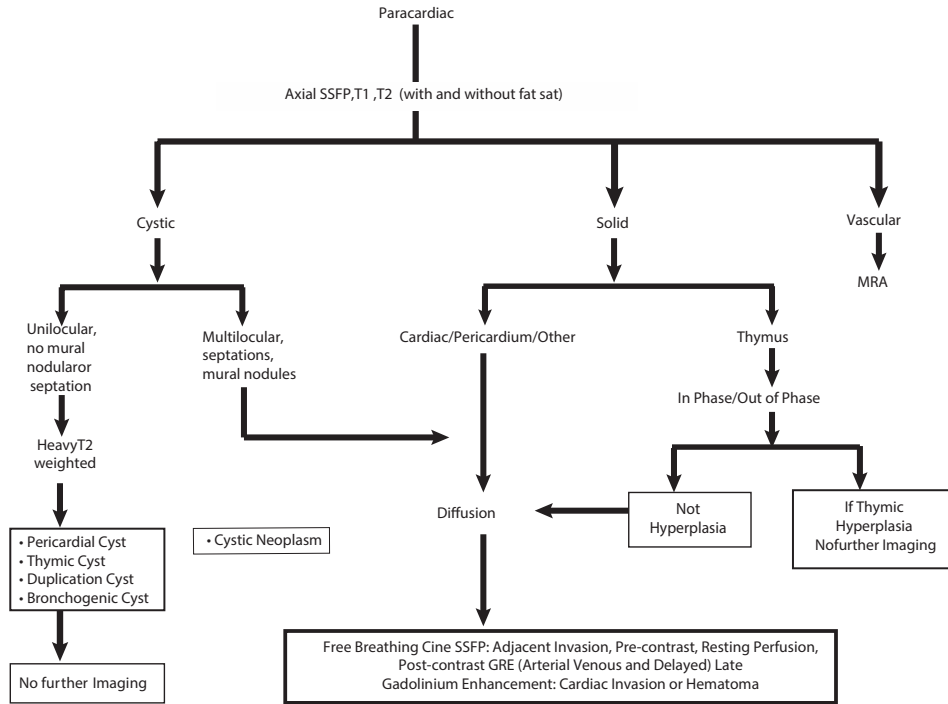
Figure 2: Flow chart illustrating an algorithmic approach for imaging the mediastinal and paracardiac lesions identified on computed tomography which may need further evaluation with magnetic resonance imaging. Contrast-enhanced magnetic resonance imaging with subtraction images are useful to identify subtle nodular or septal enhancement. In patients with acute or chronic renal failure gadolinium-based contrast agents should not be used due to the increased risk of nephrogenic systemic fibrosis.

Table 2: Imaging characteristics of benign mediastinal and pericardial lesions on MRI

Benign lesion	T1	T2	Fat saturation	Delayed enhancement	Notes
Pericardial cyst	Hypointense	Hyperintense	No fat content	Non-enhancing	Rt. cardiophrenic angle
Thymic cyst	Hypointense	Hyperintense	No fat content	Non-enhancing	Anterior mediastinum
Any cyst containing blood products	Hyperintense	Hyperintense	No fat content	Non-enhancing	Appearance depends on age of hemorrhage
Bronchogenic cyst	Hypo/hyperintense	Hyperintense	No fat content	Non-enhancing	Carina
Necrotic lymph node/abscess	Hypointense	Hyperintense	No fat content	Rim enhancing	Diffusion restriction
Vascular malformation hemangioma	Heterogeneous	Heterogeneous Hyperintense Nodular/linear hypointensities	No fat content	Heterogeneous enhancement	Pericardium
Lipoma	Hyperintense	Hyperintense	Homogenous suppression	Non-enhancing	Interatrial septum
Thymus Hyperplasia	Hypointense	Heterogeneous with hyperintense areas	No fat content	Non-cystic portion may enhance	Chemical shift ratio <0.6

the left ventricle. The presence of macroscopic fat can be confirmed using fat saturation techniques.[16]

IN PHASE/OUT OF PHASE

Differentiation of a thymic lesion that is not fluid attenuation can be challenging on CT [Figure 5, thymic hyperplasia]. Chemical shift MR imaging can be used to differentiate thymic hyperplasia from thymic tumors.[17] Thymic tissue reveals homogeneous decrease in signal intensity on opposed-phase MR images.[18] A chemical shift ratio (CSR) determined by comparing the signal intensity of the thymus gland with that of the paraspinal muscles can distinguish between thymic hyperplasia and tumors. CSR of 0.614 ± 0.130 is seen with hyperplasia compared to 1.026 ± 0.039 seen with thymic tumors.[17] Fat saturation performed with either T1W or T2-weighted (T2W) sequences saturates or reduces the signal of gross, macroscopic fat as opposed to in- and out-of-phase chemical shift MRI which suppresses the signal of microscopic fat.[16] Teratomas commonly

Table 3: Imaging characteristics of benign mediastinal and pericardial lesions on MRI

| Malignant Lesion	T1	T2	Fat saturation	Contrast enhancement	Notes
Mesothelioma	Isointense	Hyperintense	No fat content	Nodular pleural enhancement	H/o asbestos exposure
Teratoma	Fat: Hyperintense Fluid: Hypointense	Fat: Hyperintense Fluid: Hyperintense	Macroscopic fat which suppresses	Solid non calcified component enhances, in teratocarcinoma adjacent enhancement indicate invasion	calcifications on CT appear as low signal intensity on GRE
Lymphoma	Isointense	Isointense or Hyperintense	No fat content	Heterogeneous enhancement	Diffusion restriction
Neurofibroma	Isointense	Hyperintense	No fat content	Heterogeneous enhancement	Neurofibromatosis DD: Paraganglioma
Sarcoma	Heterogeneous	Heterogeneous Necrotic can be hyperintense	May contain Macroscopic fat	Heterogeneous, Solid component enhances	Invasion of adjacent structures points to sarcoma
Metastatic disease	Usually hypointense	Usually hyperintense	Depends on primary	Depends on primary	Lung, melanoma and breast
Thymic carcinoma	Heterogeneous		Focal fat	Heterogeneous enhancement	Extends from mediastinum.
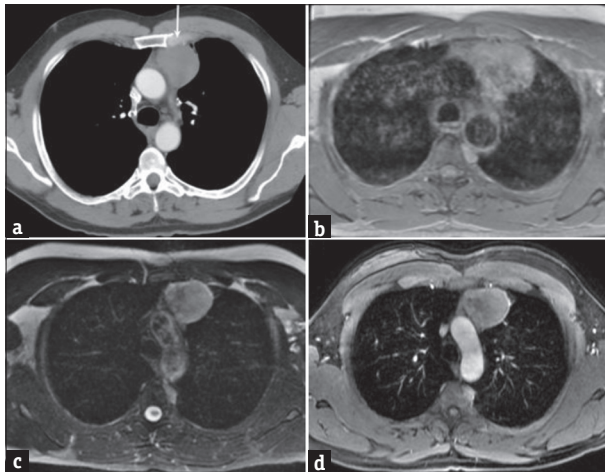
Figure 3: A 55-year-old with past medical history of the upper extremity melanoma 12 years back, now presenting with a newly discovered mediastinal mass on annual surveillance radiograph. Contrast-enhanced computed tomography (a) demonstrates an anterior mediastinal mass (white arrow). Is this a new metastasis or a primary mediastinal malignancy? Thoracic magnetic resonance imaging obtained for further characterization. T1 image (b) shows high- signal intensity. Increased signal intensity on T1-weighted images can be seen with melanin, blood and protein. T2 image (c) shows increased signal within the lesion. High T1 can be seen with melanoma. The lesion demonstrates contrast enhancement (d), excluding a hematoma or a proteinaceous cyst, and thus confirming metastatic melanoma. Another T1 hyperintense lesion was identified in the right major fissure (not shown here) consistent with metastasis. Biopsy was performed only of one lesion that confirmed melanoma.

occur in the anterior mediastinum and contain variable amount of macroscopic fat [Figure 6].

T2 WEIGHTED

T2W sequences depend on transverse relaxation and can be obtained as spin-echo, fast spin-echo, or single–shot fast spin echo (SSFSE). SSFSE is low temporal resolution but comprise of a single-breath-held
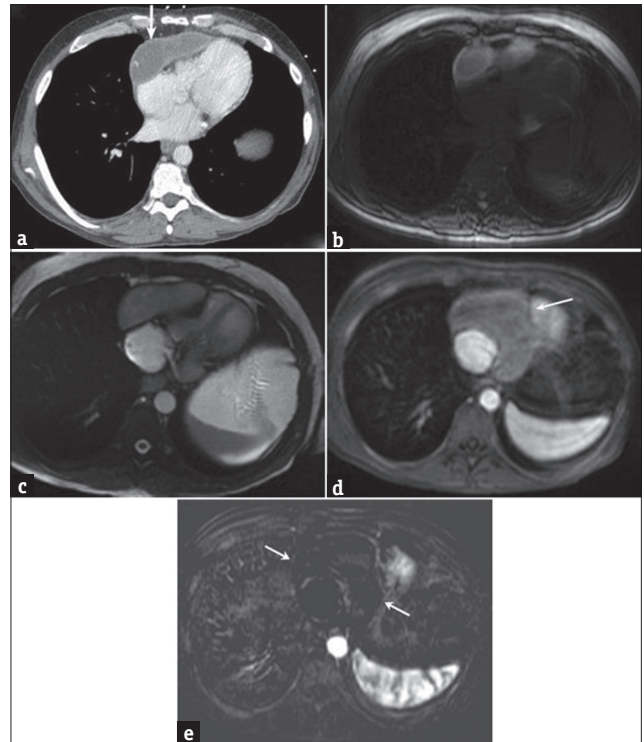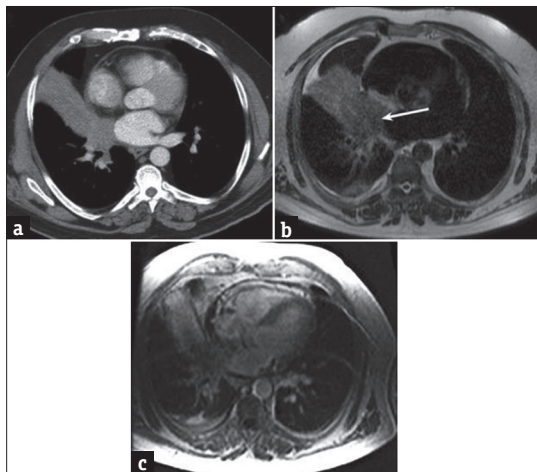

Figure 4: A 55-year-old with a history of factor X deficiency, chronic obstructive pulmonary disease, and cirrhosis being evaluated with ultrasound as part of pre-liver transplant workup, which demonstrated an incidental mediastinal mass. Contrast-enhanced computed tomography (a) obtained for further evaluation demonstrates an anterior mediastinal/pericardial lesion (white arrow). Is this benign or malignant? magnetic resonance imaging obtained for further characterization demonstrates increased signal intensity on T1 (b) and pericardial constriction on steady-state free precession (c) images. Postcontrast images (white arrows) at a more inferior level demonstrate no contrast enhancement (d: postcontrast venous phase; e: subtraction image). This is consistent with pericardial hematoma with constrictive pericarditis and this is the likely the cause of the cirrhosis. Patient underwent excision of this lesion. The properties of hematoma evolve as the lesion moves through acute, subacute, and chronic phases. See also Video 1.

acquisition. Inversion recovery or black blood sequences can be obtained to differentiate moving protons such as in blood. Water density fluid, fat, and blood can appear hyperintense on such sequences. Mediastinal invasion from paracardiac tumors can be assessed by evaluating fat planes adjacent to cardiovascular structures [Figure 7, Lung cancer T2W coronal image]. To identify intact fat planes, it is imperative not to use fat suppression for
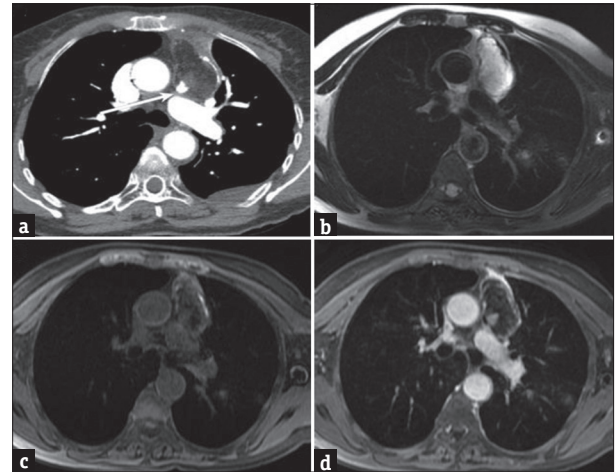
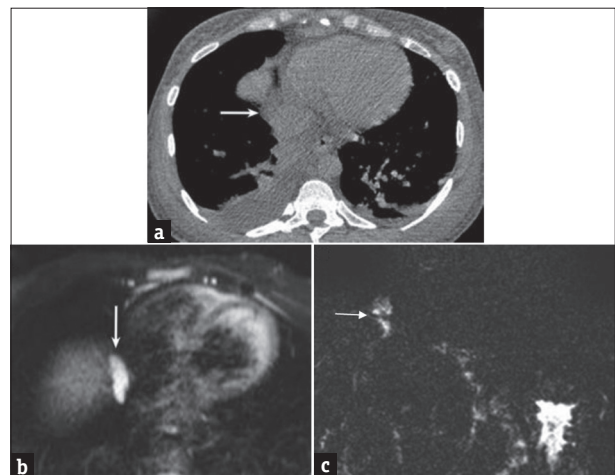such an indication. Intact and smooth fat, low-signal line between the tumor and the contact structure, and
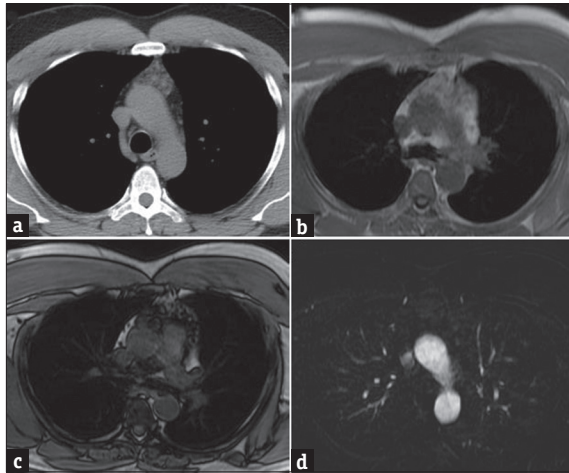
Figure 5: Noncontrast-enhanced computed tomography (a) being performed as part of metastasis work up demonstrates a nonfluid attenuating anterior mediastinal lesion (32 HU). Noncontrast magnetic resonance can be useful to differentiate benign condition such as thymic hyperplasia from thymic tumors. A chemical shift ratio is calculated by comparing the signal intensity of the thymus gland with the paraspinal muscle. b: In phase sequence, c: out of phase sequence. Postcontrast-enhanced subtraction images demonstrate no contrast enhancement (d). In this case, the chemical shift ratio = 0.60, with no contrast enhancement seen. This is consistent with thymic hyperplasia.

Figure 6: Mature Teratoma. Contrast-enhanced computed tomography (a) being performed to evaluate a mediastinal lesion identified on chest radiograph in a 50 y/o patient presenting to the emergency department with chest pain demonstrates a complex calcified fat-containing anterior mediastinal lesion suggestive of a teratoma. Fat planes with pulmonary artery were effaced raising the suspicion of adherence (white arrow). This finding is important to assess preoperatively as the surgical approach may change. If the pulmonary artery is indeed adherent, the patient may need a cardiopulmonary bypass at the time of the resection. T2-weighted axial magnetic resonance imaging (b) demonstrates heterogeneous fat suppression. What is the cause? The shim volume at the time of acquisition was too large thus only the postfat is suppressed. Precontrast T1-weighted magnetic resonance imaging (c) obtained with corrected shim volume for the acquisition demonstrates adequate fat suppression with focal nodular enhancement (d). Cine steady state-free precession demonstrates the lesion adherence to the pulmonary artery. Pericardial adherence was also confirmed at surgery and required small pericardiectomy.


Figure 7: A 60-year-old patient with newly diagnosed lung cancer. Contrast-enhanced computed tomography (a) demonstrates a right hilar mass with computed tomography findings suggestive of pericardial invasion. In addition is there cardiac invasion also? T2 image without fat suppression (b) demonstrates loss of fat plane between the lesion and pericardium and let atrium (white arrow). Steady state-free precession image (c) demonstrates direct invasion of the left atria, which was not very obvious on computed tomography. Cine steady state-free precession demonstrated the absence of the sliding sign confirming left atrial invasion.

Figure 8: Chest computed tomography being performed as part of metastatic work up in a patient with cirrhosis and hepatocellular carcinoma. Axial computed tomography (a) image demonstrates a nondependent fluid collection in the right cardiophrenic angle abutting the right atrium. Could this be a necrotic lymph node, loculated pleural effusion or a pericardial cyst? Fortunately, same day abdomen magnetic resonance imaging was also being performed. Addition of a T2 (b) image demonstrates this to be hyperintense lesion at the cardiophrenic angle. A heavily-weighted T2 weighted (c) coronal image (similar to a magnetic resonance cholangiopancreatography) confirms fluid signal intensity, a finding consistent with a pericardial cyst.

absence of tumor protrusion into the contact structure, is suggestive of absence of invasion. Capsule of cystic mediastinal lesions can be assessed on T2-weighted sequence as low-signal intensity rim measuring <2 mm. Similarly, septa are also typically <2 mm in thickness.[19] Heavily T2W sequences have been used to differentiate fluid containing lesions such as hepatic cysts from adenoma.[20] Fluid attenuation inversion recovery using a half Fourier single shot spin echo has been used in the abdominal imaging for MR Cholangiopancreatography. It has also been used to confirm fluid attenuation in hepatic cysts, thus helping in differentiation from hemangioma[21,22] without the use of i.v contrast. In our experience, nonsolid benign mediastinal lesions such as pericardial cysts [Figure 8], fluid in pericardial recesses [Figure 9], and simple thymic cyst [Figure 10] also appear homogenously hyperintense on such a heavily T2-weighted sequence.
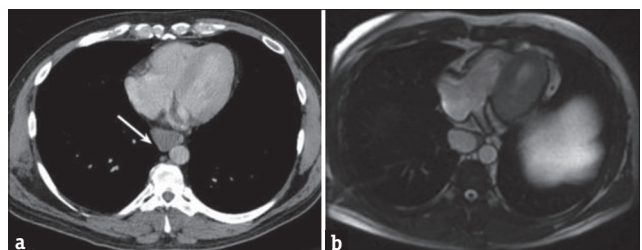
STEADY STATE FREE PRECESSION

Tissues with a high T2/T1 ratio such as fluid, fat, and blood appear bright on steady-state free precession (SSFP) sequences, but tissues with low T2/T1 such as myocardium appear dark- to-intermediate. This sequence is ideal for evaluating global and regional myocardial function, cardiac volumes, cardiac, mediastinal [Figure 11, esophageal duplication cyst], and pericardiac masses [Figure 12, neurofibroma]. The functional consequences of pericardial constriction and cardiac tamponade [Video 1] are best assessed using real-time cine SSFP sequences (diastolic collapse of the RV free wall, right atrial compression during early systole, exaggerated respiratory variation in cardiac inflow, paradoxical motion of the interventricular septum during inspiration). In addition, abnormal diastolic filling can be quantified by assessing ventricular volumes over time.[3] When this sequence is used on 3 T MRI, banding artifacts are often seen.[23] A frequency scout can identify the best phase for SSFP imaging on 3 T.[24] Breath- held ECG-gated cine MRI using SSFP technique has been found useful to evaluate direct invasion of the adjacent cardiovascular structures by identifying presence or absence of sliding motion between the mass and adjacent structures.[25] Such images are usually obtained in two orthogonal planes, perpendicular to the suspected site of invasion [Figure, 13, Video 2, cystic thymoma]. Invasion can be excluded if the mass moves without being tethered to the underlying mediastinal structures. A non-ECG-gated single-shot turbo spin echo sequence with half Fourier transformation has also been found to be very useful for evaluating local invasion by lung cancer.[26] Such a sequence can be very useful when there is poor ECG gating in the presence of arrhythmias.
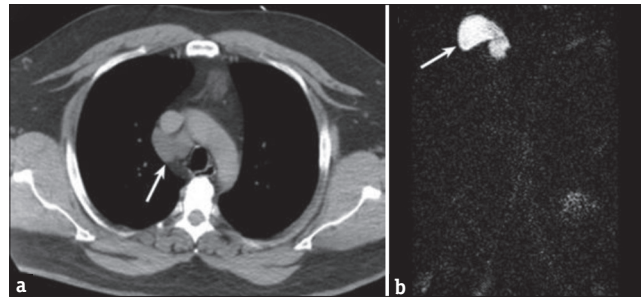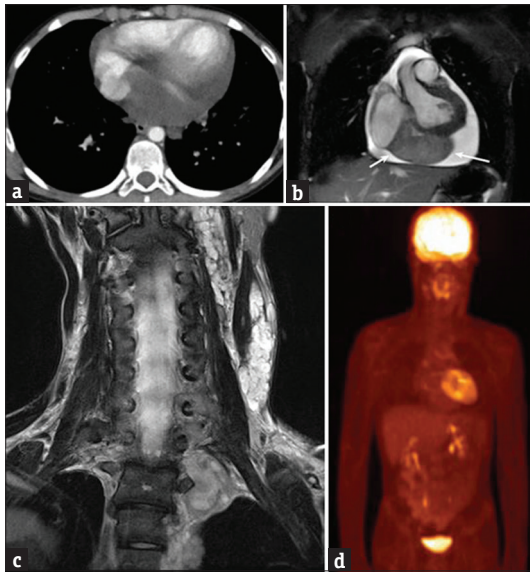

Figure 9: Axial contrast-enhanced computed tomography (a) in a patient being staged for a metastatic cancer demonstrates a hypodense lesion posterior to the superior vena cava but abutting the ascending aorta. Is this a cyst, fluid collection or a necrotic lymph node? A heavily T2-weighted sequence (b) demonstrates fluid signal intensity, which along with the location is consistent with fluid in the periaortic pericardial recess (white arrow). Less likely differential may include an atypical location for a pericardial cyst. No further follow-up or imaging is recommended.
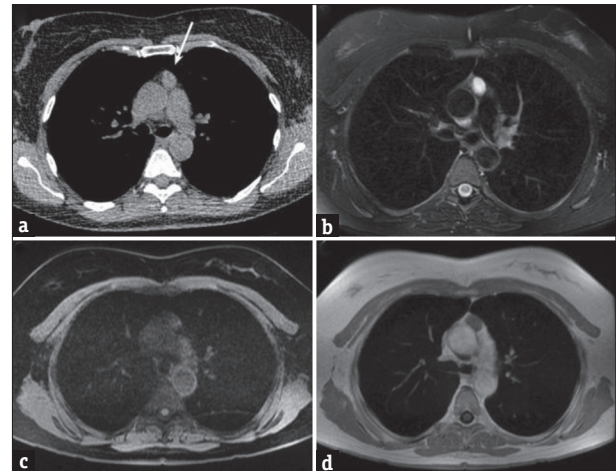
Figure 10: Low-dose noncontrast lung cancer screening computed tomography (a) in a patient with more than 25 pack years of smoking history demonstrates an anterior mediastinal lesion measuring 28 HU (white arrow). Is this a lymph node or a benign lesion such as a mediastinal cyst? T2-weighted images (b) show that this lesion has fluid signal. Fat-suppressed T1 image showingthat the lesion does not contain fat or septae (c). Postcontrast images (d) demonstrate no enhancement confirming this to be a thymic cyst. No further follow-up was needed for this.

Figure 11: Axial computed tomography (a) in a patient with chest and abdomen pain demonstrates a cystic lesion in the posterior mediastinum; this can be a lymph node or an esophageal duplication cyst (white arrow). Bright blood, steady state-free precession sequence (b) more definitively demonstrates this to be attached to the esophagus. This finding is consistent with an esophageal duplication cyst. These cysts can be lined with gastric mucosa which is prone to infection, perforation and hemorrhage.

Figure 12: A 17-year-old patient with NF1 who had been evaluated with yearly computed tomography for mediastinal neurofibromas demonstrated a slowly increasing pericardial effusion on serial contrast-enhanced computed tomography (a). Magnetic resonance imaging was requested for further characterization the pericardial effusion. Steady state-free precession (b) image clearly demonstrated a pericardial mass besides the pericardial effusion (white arrow). Imaging characteristics of this mass is similar to that of the other mediastinal, cervical (c), and cranial (not shown) lesions. This lesion had signal characteristic's similar to the other mediastinal neurofibromas. Subsequent positron emission tomography-computed tomography (d) demonstrated similar low-level uptake (SUV max of < 2) in all these lesions. This suggests a pericardial neurofibroma in addition to the increasing pericardial effusion.

Video 1: Electrocardiogram gated four-chamber cine steady-state free precession image demonstrates pericardial thickening with an organized hematoma. There is restricted motion of right atrium at right ventricle with paradoxical bowing of the ventricle septum.

REAL-TIME CINE

Dynamic respiratory MRI [Video 3, lung cancer] has been used to evaluate for tumor invasion into the chest wall or pleura.[27] These images are obtained using a snapshot fast-field echo with 25–30 images obtained while the patient takes deep breath in and out. Real-time imaging sequences tend to have low spatial resolution, but high temporal resolution which is useful for assessment of rapid physiologic changes. Imaging plane is prescribed perpendicular to the site of suspected invasion. When assessing for lung cancer invasion into chest wall or mediastinum, usually no ECG gating is
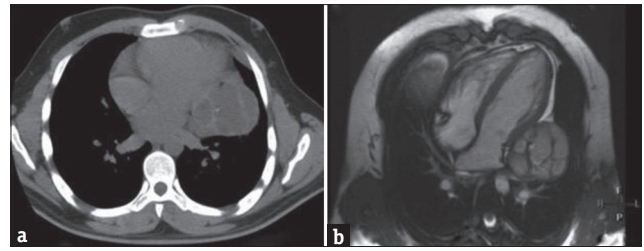
Figure 13: A 54-year-old patient presenting with chest pain in the ED. Chest radiograph demonstrated a mediastinal mass. Noncontrast computed tomography (a) obtained to better delineate this finding demonstrates a solid cystic lesion. Contrast medium could not be administered due to acute on chronic renal failure. A noncontrast magnetic resonance imaging was requested to evaluate for mediastinal invasion. steady state-free precession (b, Video 2) demonstrates the presence of sliding movement between this lesion and left ventricle, thus excluding invasion. Overlying pericardium, however, did not demonstrate sliding motion, raising the possibility of pericardial adherence which was confirmed at the time of surgery. Pathology demonstrated a cystic thymoma.

Video 2: Breath held axial cine steady-state free precession image demonstrates a (paracardiac cystic lesion with focal adherence to the pericardium. However, the underlying left ventricle is moves freely confirming lack of myocardial invasion.
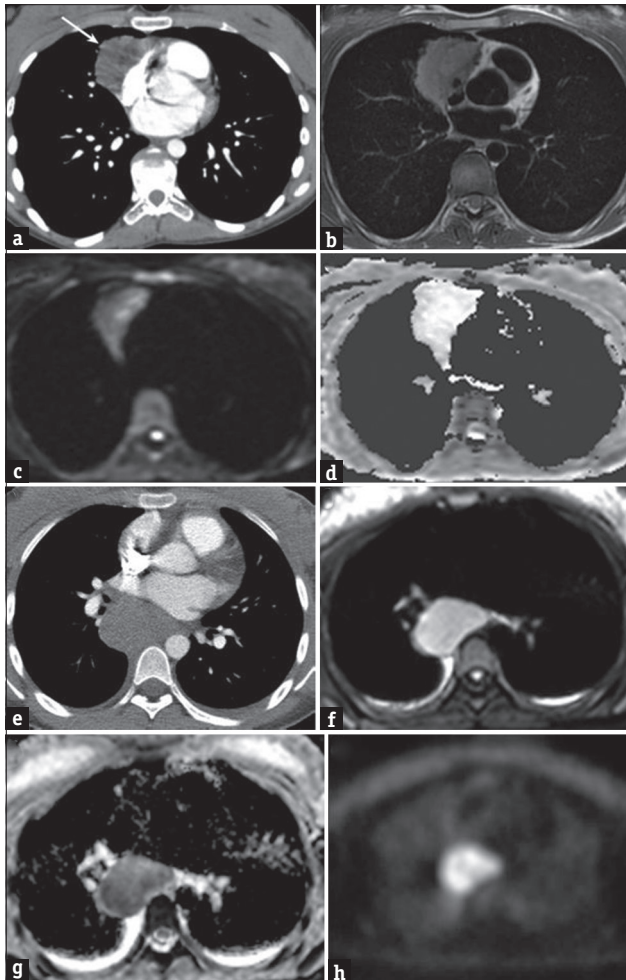

Video 3: Dynamic real-time cine magnetic resonance imaging in a patient with lung cancer and suspected myocardial invasion on computed tomography clearly identifies unrestricted sliding motion of the left ventricle while the pericardium demonstrates restricted motion and adherence to the lung cancer.

needed. Five-to-eight images maybe obtained to assess the site of invasion. Similar to cine SSFP, the presence of sliding motion implies absence of invasion while restricted motion suggests invasion. These sequences have been found to be very useful in evaluating pericardial constriction also.[3]

DIFFUSION-WEIGHTED IMAGING

Diffusion of water molecules in malignant tumors

is usually restricted compared to that in normal tissue, resulting in a decreased apparent diffusion coefficient (ADC) value in malignant lesions. Calculation of this ADC value can be used to differentiate benign from malignant mediastinal lesions. Diffusion-weighted imaging (DWI) images can be obtained as multislice single shot nonbreathold spin echo EPI. Respiratory trigger or breath hold can also be used with the diffusion gradient applied to three orthogonal directions (x, y and z). A frequency selective radiofrequency pulse is applied before the DWI pulse to obtain fat saturation. Necrosis, inflammation, and

benign lesions are characterized by increased diffusivity, and thereby higher ADC values. Different thresholds have been suggested to identify benignity using a 1.5 T MRI; ADC value of >1.22×10^{-3} mm²/s for lymph nodes,[28] 1.56×10^{-3} mm²/s for mediastinal tumors,[29] and also 1.85×10^{-3} mm²/s[30] [Figure 14, lymphoma]. Malignant lymph nodes are more likely to appear hypointense than hyper or mixed intensity on these ADC maps. High B value DWI images with ADC >2.5×10^{-3} mm²/s can help distinguish benign cysts from cystic neoplasms.[31] In patients with lung cancer, DWI imaging can also help differentiate malignant lymph nodes with an optimal 1.70×10^{-3} mm²/s.[32] ADC value is measured by placing a region of interest (ROI) either on a single slice, multiple slices or the entire volume. It is preferable to measure the ADC by placing the ROI over the solid portion of the lesion. Whole tissue volume measurements method of placing the ROI provides the most reproducible ADC values.[33] Perfusion-free ADC measurements improve diagnostic accuracy of diffusion-weighted MRI in differentiating benign conditions from malignancies of the anterior mediastinum with an ADC cutoff of 1.52×10^{-3} mm²/s.[34]

DYNAMIC CONTRAST-ENHANCED MAGNETIC RESONANCE IMAGING

Dynamic contrast-enhanced MRI is obtained as a volumetric 3D gradient recalled echo sequence. Initial noncontrast phase is followed by arterial, venous, and delayed phases using a breath hold after administration of gadolinium-based contrast agent. These images
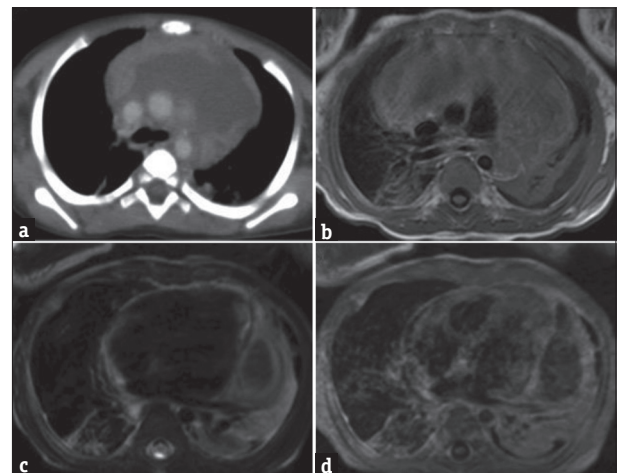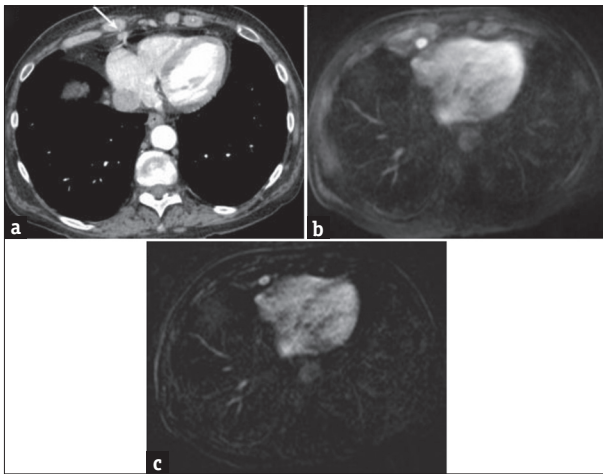

Figure 14: A 23-year-old patient presenting with chest pain. Axial contrast-enhanced computed tomography (a) obtained in the emergency department demonstrates a mediastinal mass. With prior history of treated lymphoma, this was concerning for recurrence. What else can imaging tell without doing a biopsy? Diffusion-weighted magnetic resonance imaging (b: B value of 0, C: B value of 50 and c: B value of 500) demonstrated restricted diffusion with an ADC value of < 1.39×10 (-3) mm²/s, indicating a malignant lesion, which was confirmed on biopsy. Measurement of ADC can be used to identify lymphoma that will response to treatment and also to assess response to treatment. Contrast-enhanced computed tomography (e) in a different 16-year-old patient demonstrating a subcarinal lesion. Is this a bronchogenic cyst or an enlarged lymph node? Restricted diffusion identified confirming this to be a lymph node (diffusion-weighted imaging [f], ADC map [g]). Increased fluoro-D-glucose uptake is noted on the concurrent positron emission tomography magnetic resonance imaging (h).
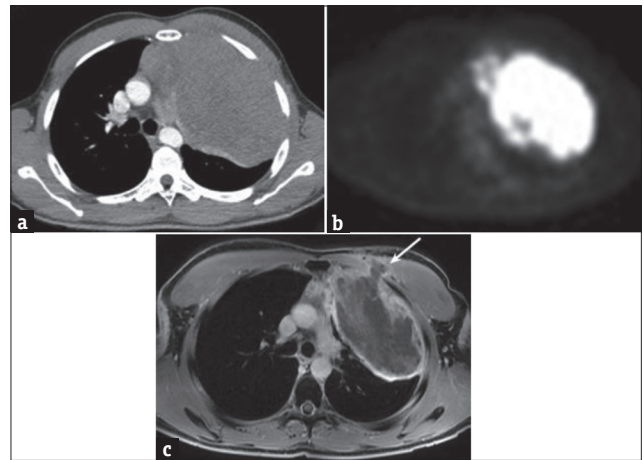

Figure 15: A 2-year-old patient with septicemia presenting to the ED, radiograph of thorax depicted a widened mediastinum. Contrast enhanced computed tomography (a) demonstrated a mediastinal mass. Initial computed tomography-guided biopsy was nondiagnostic. Magnetic resonance imaging was obtained for further characterization. T1 (b) and T2 (c, slightly lower) images demonstrate a predominantly cystic collection was heterogeneous enhancement a thickened, irregular rim. Enhanced (d) image demonstrates rim enhancement, consistent with an abscess.

are useful to identify solid from necrotic regions in a heterogeneous mediastinal mass or abscess [Figure 15]. Some researchers have also used additional phases, which are useful for obtaining time signal intensity curves.[19] Malignant lymph nodes tend to demonstrate early enhancement with slow decrease [Figure 16, metastasis from hepatocellular carcinoma] versus granulomatous lymph nodes demonstrating delayed enhancement.[35] A washout pattern has been described in patients with thymic epithelial tumors versus a persistent or plateau pattern in thymoma [Figure 17 chest wall by thymoma], thymic carcinoma, lymphoma,
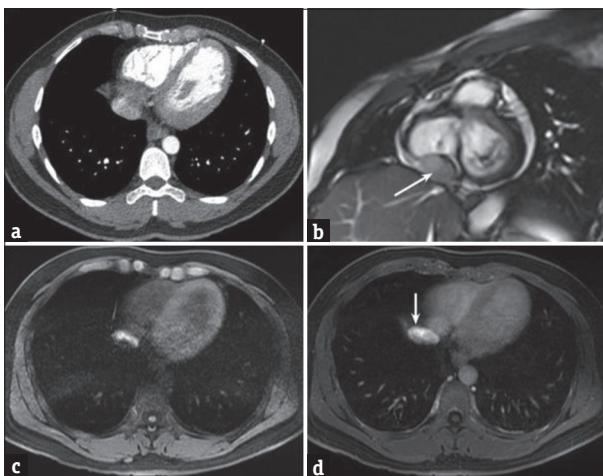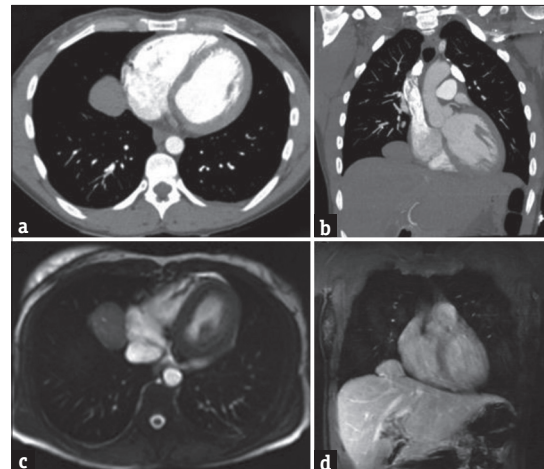

Figure 16: Axial staging contrast enhanced computed tomography (a) demonstrates a prominent cardiophrenic lymph node in a patient with known hepatocellular carcinoma. Is this benign or malignant? Arterial phase postcontrast (b) and subtraction images (c) of dynamic contrast-enhanced magnetic resonance demonstrate arterial washing similar to primary hepatic cancer. This finding was later confirmed with a positron emission tomography which also which demonstrated increased fluoro-D-glucose uptake.

Figure 18: Staging contrast-enhanced computed tomography in a patient with colon cancer demonstrates (a) a pericardial mass. This is an unusual location for an oligometastasis. Short-axis steady-state free precession (b) image demonstrating a pericardial lesion separate from the pericardial effusion and separate from the myocardium (white arrow). Pre- (c) and post-contrast (d) images demonstrating slow peripheral filling and persistent enhancement, consistent with a hemangioma. (white arrow).

and germ cell tumors.[19] Dynamic-enhanced CT has been used to identify a mediastinal hemangioma[36] and a similar sequence can also be used with MRI to identify these lesions [Figure 18, hemangioma]. Herniation of liver through a diaphragmatic defect can mimic a paracardiac mass; however, identification of enhancement pattern similar to rest of the liver parenchyma can be used to correctly identify such a lesion [Figure 19 hepatic herniation]. These sequences

Figure 17: Noncontrast computed tomography (a) demonstrates a large mass involving the mediastinum and abutting the left chest wall. With focal anterior chest wall pain, there was concern for chest wall invasion not identified on computed tomography. Staging positron emission tomography-computed tomography (b) demonstrates intense fluoro-D-glucose uptake, but still no focal anterior chest wall enhancement. Postcontrast delayed phase magnetic resonance imaging (c) with fat suppression shows that the lesion is invading the chest wall. This is the incremental value of magnetic resonance imaging over computed tomography and positron emission tomography.

Figure 19: Surveillance contrast computed tomography scan in a patient with a history of renal cell carcinoma demonstrates a right paracardiac lesion (a: axial, b: coronal). Is this a new metastasis? With recent history of trauma, a complication of trauma was also suspected. On noncontrast steady-state free precession (c) and delayed postcontrast (d) magnetic resonance images the signal intensity of this lesion is similar to adjacent liver parenchyma. On the coronal image, a hepatic vein branch can also be seen traversing the diaphragmatic defect, thus confirming this to be a postblunt trauma, diaphragmatic injury with focal hepatic herniation.

can also be used to better assess paracardiac vascular lesions such as paraesophageal varix [Figure 20], aneurysms, pseudoaneurysms, arterial, venous, or arteriovenous malformations also. Supplementation of DWI by DC-MRI may help in differentiation of benign from malignant pleural disease.[37] Invasion of adjacent structures can be identified by irregular interface between the mass and adjacent structures, protrusion into adjacent structures, or enhancement of the contact structure [Figure 17 chest wall by thymoma]. Contrast-enhanced MRI can demonstrate the nodular enhancement, similar to the fluoro-D-glucose uptake on positron emission tomography-CT, seen with mesothelioma that can be difficult to identify on CT [Figure 21].

First Pass Perfusion

Resting perfusion images have been used in cardiac imaging to identify the regions of decreased perfusion. In neuroimaging, these images are often used for stroke protocol to identify brain parenchyma with decreased perfusion. This sequence thus helps identify tissue at risk for infarction and has both cardiac[38] and brain[39] applications. In addition, perfusion imaging of brain tumors[40] is routinely performed to identify the patterns of enhancement and assess response to treatment. More recently, perfusion imaging has been used for assessment of hepatocellular carcinoma[41] and renal cell cancer.[42,43] In future, similar imaging techniques may find potential uses in assessment of mediastinal and paracardiac tumors. An additional advantage of a perfusion sequence

is to identify if the paracardiac lesion is vascular in origin and communicates either with the cardiac chambers or coronary vessels.[44]

Delayed Enhanced

Postgadolinium-enhanced MRI is increasingly being used to identify scar from ischemic heart diseases, cardiomyopathy, and intracavitary thrombus.[45,46] Thrombus is avascular, therefore, there is no gadolinium uptake. With long-inversion-time imaging (Inversion time = 600 ms), regions with normal contrast uptake such as viable myocardium increase in signal intensity appearing gray, whereas thrombus appears homogeneously dark as there is no gadolinium uptake.[47] In our experience, similar imaging appearance can be seen with mediastinal or pericardial hematomas, which are avascular [Figure 22]. Care must be taken while interpreting these as peripheral enhancement can be seen due to associated pericarditis.

Conclusion

CT is often the diagnostic modality of choice for identification of mediastinal lesions and most often
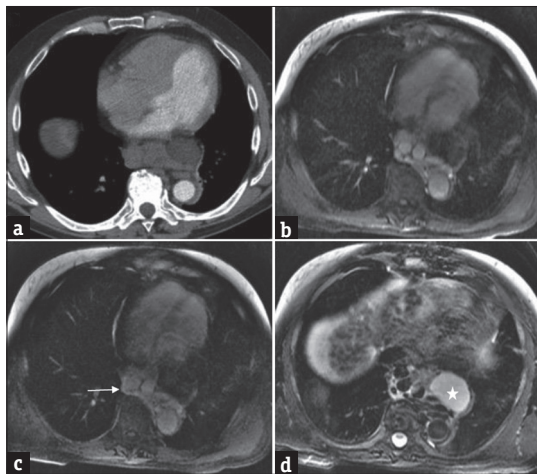
Figure 20: Surveillance contrast-enhanced computed tomography (a) in a patient with a history of hepatocellular carcinoma and liver transplant demonstrates tubular and cystic structures abutting the esophagus. Are these all paraesophageal venous varix? Postcontrast enhanced venous and delayed phase (b and c) magnetic resonance imaging demonstrate enhancement in the tubular structures consistent with varix. A hypointense lesion remains nonenhancing on delayed (white arrow) confirming these to be dilated veins in most of these except for the cystic lesion. Axial respiratory triggered T2 (d) demonstrates fluid signal intensity in this cystic lesion (star). This is likely abdomen ascites in the small paraesophageal hernia sac.
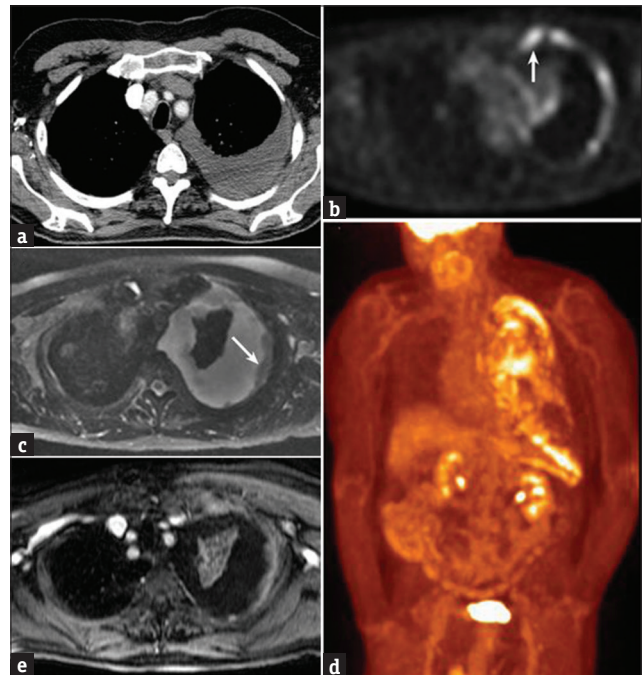
Figure 21: Mesothelioma. Axial contrast-enhanced computed tomography (a) in a patient with slowly increasing left pleural effusion demonstrates subtle posterior nodularity concerning for malignant effusion. Axial T2-weighted (b) and contrast enhanced (c) magnetic resonance imaging clearly identified nodular thickening of the costal and mediastinal pleura suspicious for a malignancy (white arrow). Thoracentesis and pleural biopsy confirmed the diagnosis of mesothelioma. Subsequently obtained positron emission tomography-computed tomography (d) demonstrates diffuse and focal pleural fluoro-D-glucose uptake which is similar to the contrast enhanced magnetic resonance imaging (e). In addition, focal extension into the intercostal space anteriorly is also seen (c, arrow).
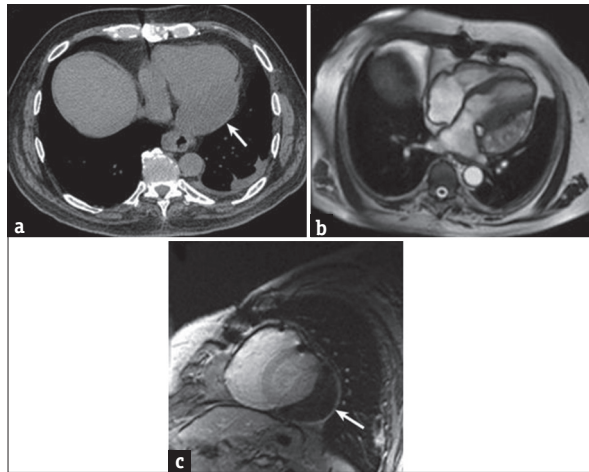
Figure 22: Axial computed tomography (a) in a patient with hepatocellular carcinoma left paracardiac mass. Is this benign or malignant? steady state-free precession sequence (b) from magnetic resonance imaging demonstrates heterogeneous signal intensity. Postcontrast delayed enhanced image at a longer inversion time (600 ms) demonstrates no enhancement (c) in this (white arrow). This is consistent with a pericardial organized hematoma/thrombus.

answers most of the clinical questions. However, there is incremental value of MRI for further characterization of paracardiac mediastinal lesions considered indeterminate on CT or when confirmation of tumor invasion into adjacent structures is needed. MRI is emerging as a tool for "virtual biopsy" for mediastinal masses and may become an important imaging modality to assess early tumor response to treatment, preceding diminution of tumor size. These very sick patients may not be able to perform breath holds required for multiple sequences. Protocols for each exam should be individualized to optimize diagnostic yield in context of the magnified time constraints in these patients. A judicious and tailored approach to imaging this subset of patients will be instrumental towards building a successful thoracic MRI practice that looks beyond the cardiac indications of thoracic MRI.

Financial support and sponsorship

Conflicts of interest

There are no conflicts of interest.

References

1. Bogaert J, Francone M. Pericardial disease: Value of CT and MR imaging. Radiology 2013;267:340-56.
2. Hoffmann U, Globits S, Schima W, Loewe C, Puig S, Oberhuber G, et al. Usefulness of magnetic resonance imaging of cardiac and paracardiac masses. Am J Cardiol 2003;92:890-5.
3. Rajiah P. Cardiac MRI: Part 2, pericardial diseases. AJR Am J Roentgenol 2011;197:W621-34.
4. Jeung MY, Gasser B, Gangi A, Bogorin A, Charneau D, Wihlm JM, et al. Imaging of cystic masses of the mediastinum. Radiographics 2002;22:S79-93.
5. Whitten CR, Khan S, Munneke GJ, Grubnic S. A diagnostic approach to mediastinal abnormalities. Radiographics 2007;27:657-71.
6. Carter BW, Benveniste MF, Madan R, Godoy MC, de Groot PM, Truong MT, et al. ITMIG classification of mediastinal compartments and multidisciplinary approach to mediastinal masses. Radiographics 2017;37:413-36.
7. Gray H. Anatomy of the Human Body. 20th ed. Philadelphia: W.H. Lewis; 2000.
8. Spodick DH. Macrophysiology, microphysiology, and anatomy of the per icardium: A synopsis. Am Heart J 1992;124:1046-51.
9. Groell R, Schaffler GJ, Rienmueller R. Pericardial sinuses and recesses: Findings at electrocardiographically triggered electron-beam CT. Radiology 1999;212:69-73.
10. Talbot BS, Weinberg EP. MR imaging with metal-suppression sequences for evaluation of total joint arthroplasty. Radiographics 2016;36:209-25.
11. Murayama S, Murakami J, Watanabe H, Sakai S, Hinaga S, Soeda H, et al. Signal intensity characteristics of mediastinal cystic masses on T1-weighted MRI. J Comput Assist Tomogr 1995;19:188-91.
12. Ginat DT, Meyers SP. Intracranial lesions with high signal intensity on T1-weighted MR images: Differential diagnosis. Radiographics 2012;32:499-516.
13. Isiklar I, Leeds NE, Fuller GN, Kumar AJ. Intracranial metastatic melanoma: Correlation between MR imaging characteristics and melanin content. AJR Am J Roentgenol 1995;165:1503-12.
14. Rabkin SW. Epicardial fat: Properties, function and relationship to obesity. Obes Rev 2007;8:253-61.
15. Wang ZJ, Reddy GP, Gotway MB, Yeh BM, Hetts SW, Higgins CB, et al. CT and MR imaging of pericardial disease. Radiographics 2003;23:S167-80.
16. Ackman JB. A practical guide to nonvascular thoracic magnetic resonance imaging. J Thorac Imaging 2014;29:17-29.
17. Inaoka T, Takahashi K, Mineta M, Yamada T, Shuke N, Okizaki A, et al. Thymic hyperplasia and thymus gland tumors: Differentiation with chemical shift MR imaging. Radiology 2007;243:869-76.
18. Takahashi K, Inaoka T, Murakami N, Hirota H, Iwata K, Nagasawa K, et al. Characterization of the normal and hyperplastic thymus on chemical-shift MR imaging. AJR Am J Roentgenol 2003;180:1265-9.
19. Yabuuchi H, Matsuo Y, Abe K, Baba S, Sunami S, Kamitani T, et al. Anterior mediastinal solid tumours in adults: Characterisation using dynamic contrast-enhanced MRI, diffusion-weighted MRI, and FDG-PET/CT. Clin Radiol 2015;70:1289-98.
20. Mortelé KJ, Ros PR. Cystic focal liver lesions in the adult: Differential CT and MR imaging features. Radiographics 2001;21:895-910.
21. Sasaki K, Ito K, Koike S, Fujita T, Okazaki H, Matsunaga N, et al. Differentiation between hepatic cyst and hemangioma: Additive value of breath-hold, multisection fluid-attenuated inversion-recovery magnetic resonance imaging using half-fourier acquisition single-shot turbo-spin-echo sequence. J Magn Reson Imaging 2005;21:29-36.
22. Kiryu S, Okada Y, Ohtomo K. Differentiation between hemangiomas and cysts of the liver with single-shot fast-spin echo image using short and long TE. J Comput Assist Tomogr 2002;26:687-90.
23. Oshinski JN, Delfino JG, Sharma P, Gharib AM, Pettigrew RI. Cardiovascular magnetic resonance at 3.0 T: Current state of the art. J Cardiovasc Magn Reson 2010;12:55.
24. Rajiah P, Bolen MA. Cardiovascular MR imaging at 3 T: Opportunities, challenges, and solutions. Radiographics 2014;34:1612-35.
25. Seo JS, Kim YJ, Choi BW, Choe KO. Usefulness of magnetic resonance imaging for evaluation of cardiovascular invasion:

Evaluation of sliding motion between thoracic mass and adjacent structures on cine MR images. J Magn Reson Imaging 2005;22:234-41.

26. Chang S, Hong SR, Kim YJ, Hong YJ, Hur J, Choi BW, et al. Usefulness of thin-section single-shot turbo spin echo with half-fourier acquisition in evaluation of local invasion of lung cancer. J Magn Reson Imaging 2015;41:747-54.

27. Akata S, Kajiwara N, Park J, Yoshimura M, Kakizaki D, Abe K, et al. Evaluation of chest wall invasion by lung cancer using respiratory dynamic MRI. J Med Imaging Radiat Oncol 2008;52:36-9.

28. Abdel Razek AA, Gaballa G, Elashry R, Elkhamary S. Diffusion-weighted MR imaging of mediastinal lymphadenopathy in children. Jpn J Radiol 2015;33:449-54.

29. Razek AA, Elmorsy A, Elshafey M, Elhadedy T, Hamza O. Assessment of mediastinal tumors with diffusion-weighted single-shot echo-planar MRI. J Magn Reson Imaging 2009;30:535-40.

30. Abdel Razek AA, Elkammary S, Elmorsy AS, Elshafey M, Elhadedy T. Characterization of mediastinal lymphadenopathy with diffusion-weighted imaging. Magn Reson Imaging 2011;29:167-72.

31. Shin KE, Yi CA, Kim TS, Lee HY, Choi YS, Kim HK, et al. Diffusion-weighted MRI for distinguishing non-neoplastic cysts from solid masses in the mediastinum: Problem-solving in mediastinal masses of indeterminate internal characteristics on CT. Eur Radiol 2014;24:677-84.

32. Usuda K, Sagawa M, Motono N, Ueno M, Tanaka M, Machida Y, et al. Advantages of diffusion-weighted imaging over positron emission tomography-computed tomography in assessment of hilar and mediastinal lymph node in lung cancer. Ann Surg Oncol 2013;20:1676-83.

33. Priola AM, Priola SM, Parlatano D, Gned D, Giraudo MT, Giardino R, et al. Apparent diffusion coefficient measurements in diffusion-weighted magnetic resonance imaging of the anterior mediastinum: Inter-observer reproducibility of five different methods of region-of-interest positioning. Eur Radiol 2017;27:1386-94.

34. Priola AM, Priola SM, Gned D, Piacibello E, Sardo D, Parvis G, et al. Diffusion-weighted quantitative MRI to diagnose benign conditions from malignancies of the anterior mediastinum: Improvement of diagnostic accuracy by comparing perfusion-free to perfusion-sensitive measurements of the apparent diffusion coefficient. J Magn Reson Imaging 2016;44:758-69.

35. Laissy JP, Gay-Depassier P, Soyer P, Dombret MC, Murciano G, Sautet A, et al. Enlarged mediastinal lymph nodes in bronchogenic carcinoma: Assessment with dynamic contrast-enhanced MR imaging. Work in progress. Radiology 1994;191:263-7.

36. Okasaka T, Iwano S, Usami N, Uchiyama M, Sato N, Ito S, et al. Usefulness of dynamic computed tomography for the diagnosis of mediastinal hemangioma. Kyobu Geka 2007;60:1031-4.

37. Coolen J, De Keyzer F, Nafteux P, De Wever W, Dooms C, Vansteenkiste J, et al. Malignant pleural disease: Diagnosis by using diffusion-weighted and dynamic contrast-enhanced MR imaging – Initial experience. Radiology 2012;263:884-92.

38. Gerber BL, Raman SV, Nayak K, Epstein FH, Ferreira P, Axel L, et al. Myocardial first-pass perfusion cardiovascular magnetic resonance: History, theory, and current state of the art. J Cardiovasc Magn Reson 2008;10:18.

39. Petrella JR, Provenzale JM. MR perfusion imaging of the brain: Techniques and applications. AJR Am J Roentgenol 2000;175:207-19.

40. Provenzale JM, Mukundan S, Barboriak DP. Diffusion-weighted and perfusion MR imaging for brain tumor characterization and assessment of treatment response. Radiology 2006;239:632-49.

41. Taouli B, Johnson RS, Hajdu CH, Oei MT, Merad M, Yee H, et al. Hepatocellular carcinoma: Perfusion quantification with dynamic contrast-enhanced MRI. AJR Am J Roentgenol 2013;201:795-800.

42. Jeon TY, Kim CK, Kim JH, Im GH, Park BK, Lee JH, et al. Assessment of early therapeutic response to sorafenib in renal cell carcinoma xenografts by dynamic contrast-enhanced and diffusion-weighted MR imaging. Br J Radiol 2015;88:20150163.

43. Kang HC, Tan KS, Keefe SM, Heitjan DF, Siegelman ES, Flaherty KT, et al. MRI assessment of early tumor response in metastatic renal cell carcinoma patients treated with sorafenib. AJR Am J Roentgenol 2013;200:120-6.

44. Chaturvedi A, Vummidi D, Shuman WP, Dubinsky TJ, Maki JH. Cardiac angiosarcoma: An unusual cause of coronary artery pseudoaneurysm. J Thorac Imaging 2012;27:W8-9.

45. Vogel-Claussen J, Rochitte CE, Wu KC, Kamel IR, Foo TK, Lima JA, et al. Delayed enhancement MR imaging: Utility in myocardial assessment. Radiographics 2006;26:795-810.

46. Mollet NR, Dymarkowski S, Volders W, Wathiong J, Herbots L, Rademakers FE, et al. Visualization of ventricular thrombi with contrast-enhanced magnetic resonance imaging in patients with ischemic heart disease. Circulation 2002;106:2873-6.

47. Weinsaft JW, Kim HW, Shah DJ, Klem I, Crowley AL, Brosnan R, et al. Detection of left ventricular thrombus by delayed-enhancement cardiovascular magnetic resonance prevalence and markers in patients with systolic dysfunction. J Am Coll Cardiol 2008;52:148-57.